The Meteoritical Society

Meteoritics & Planetary Science 53, Nr 11, 2395–2412 (2018)
doi: 10.1111/maps.13136

Aqueous alteration of the Martian meteorite Northwest Africa 817: Probing fluid–rock interaction at the nakhlite launch site

M. R. LEE[1,*], L. DALY[1], B. E. COHEN[1,2], L. J. HALLIS[1], S. GRIFFIN[1], P. TRIMBY[3], A. BOYCE[2], and D. F. MARK[2]

[1]School of Geographical and Earth Sciences, University of Glasgow, Gregory Building, Lilybank Gardens, Glasgow G12 8QQ, UK
[2]Scottish Universities Environmental Research Centre, Rankine Avenue, Scottish Enterprise Technology Park, East Kilbride G75 0QF, UK
[3]Oxford Instruments Nanoanalysis, High Wycombe HP12 3SE, UK
[*]Corresponding author. E-mail: martin.lee@glasgow.ac.uk

(Received 08 March 2018; revision accepted 22 May 2018)

Abstract–The nakhlite meteorites characteristically contain iddingsite, a hydrous iron–magnesium silicate that formed by aqueous alteration on Mars. Iddingsite is most abundant in Northwest Africa (NWA) 817, and alteration products in this meteorite also have the lowest deuterium/hydrogen ratio of any nakhlite. Taken together, these distinctive properties could be interpreted to show that NWA 817 was altered under different physico-chemical conditions than the other nakhlites and by liquid water from a separate reservoir. Here this interpretation is tested through a petrographic, mineralogical, chemical, and isotopic study of NWA 817. We find that its iddingsite occurs as olivine-hosted veins of nanocrystalline smectite and Fe-oxyhydroxide. Strong similarities in the mineralogy of iddingsite between NWA 817 and other nakhlites suggest that these meteorites were altered under comparable physico-chemical conditions, with the Fe-rich composition of NWA 817 olivine grains rendering them especially susceptible to aqueous alteration. Analyses of NWA 817 bulk samples by stepwise pyrolysis confirm that its iddingsite has unusually low deuterium/hydrogen ratios, but owing to terrestrial weathering of this meteorite, the hydrogen isotopic data cannot be used with confidence to infer the origin of Martian aqueous solutions. NWA 817 was most probably altered along with the other nakhlites over a short time period and in a common aqueous system. One interpretation of a correlation between the eruption ages of three of the nakhlites and the chemical composition of their iddingsite is that water originated from close to the surface of Mars and flowed through the nakhlite lava pile under the influence of gravity.

INTRODUCTION

Meteorites of the nakhlite group sample the mid-Amazonian igneous crust of Mars (e.g., Bogard and Johnson 1983; McSween 1994; Nyquist et al. 2001). Strong similarities between them in bulk chemical composition, mineralogy, and cosmic ray exposure age indicates that these meteorites were impact-ejected simultaneously, and from the same place on Mars's surface (e.g., Treiman 2005). The launch site has been suggested to contain a single thick lava flow/intrusion (e.g., Friedman-Lentz et al. 1999; Mikouchi et al. 2006, 2012; Corrigan et al. 2015), or multiple lavas (Jambon et al. 2016). Recent $^{40}Ar/^{39}Ar$ dating of six meteorites indicates that they were sourced from at least four lava flows that formed over a time span of ~93 Ma (i.e., between 1416 ± 7 Ma and 1322 ± 10 Ma; Cohen et al. 2017).

The nakhlites are composed principally of augite and olivine phenocrysts, between which is a finely crystalline (rarely glassy) mesostasis (Bunch and Reid 1975). Most of them also contain a very fine-grained material called iddingsite (Ashworth and Hutchison 1975) (Fig. 1), whose constituents include hydrous

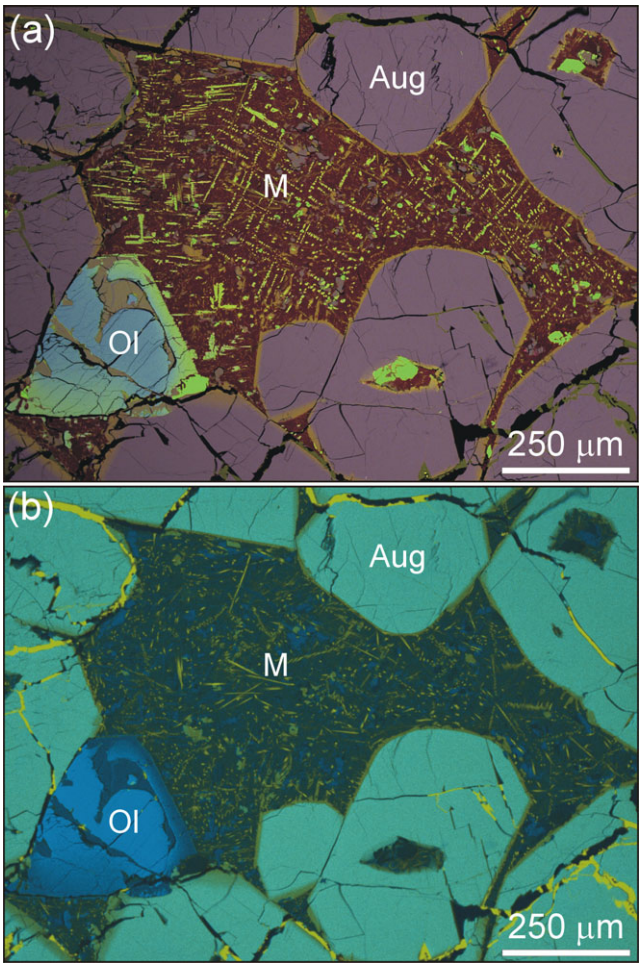

Fig. 1. An area of N8-1 containing augite (Aug), olivine (Ol), and mesostasis (M). a) X-ray map overlain on a BSE image. The X-ray map has been made by blending three element maps: Si Kα (red), Mg Kα (blue), and Fe Kα (green). These color combinations render augite grain cores purple, the narrow Fs-rich rims to augite grains orange, olivine grain cores blue, olivine grain rims light green, iddingsite brown, equant grains of Fe-Ti oxide lime green, and the mesostasis predominantly dark red. Both the augite and olivine grains are compositionally zoned, and the mesostasis contains many acicular Fe-rich crystals. b) X-ray map of the same field of view as (a) that was made by blending maps for Mg Kα (blue) and Ca Kα (yellow). This element combination renders olivine mid blue to dark blue, augite turquoise, calcite yellow. Open fractures are black, and the mesostasis contains a variety of fine crystals. Note that the calcite veins are almost entirely restricted to augite. (Color figure can be viewed at wileyonlinelibrary.com.)

silicates (smectite, serpentine, opal-A, amorphous gel, stilpnomelane), Fe-oxides, and Fe-oxyhydroxides (Bunch and Reid 1975; Gooding et al. 1991; Treiman et al. 1993; Bridges and Grady 2000; Gillet et al. 2002; Noguchi et al. 2009; Changela and Bridges 2011; Chatzitheodoridis et al. 2014; Kuebler 2013; Lee et al. 2013, 2015a; Lee and Chatzitheodoridis 2016). The iddingsite is commonly intergrown with siderite, gypsum, and halite (e.g., Gooding et al. 1991; Bridges and Grady 2000; Lee et al. 2013; Tomkinson et al. 2013). As iddingsite has formed from aqueous solutions, its presence in the nakhlites shows that liquid water must have been available in the crust of Mars relatively late in the planet's history (Ashworth and Hutchison 1975).

The origin of the aqueous fluids that were responsible for alteration of the nakhlites can be constrained using the hydrogen isotopic composition of water/OH in iddingsite because various reservoirs of Martian hydrogen differ in their deuterium/hydrogen (D/H) ratio (hereafter expressed as δD $[(D/H)_{sample}/(D/H)_{V\text{-}SMOW} - 1] \times 1000$). The planet's atmosphere is D-rich (present-day δD is 4950 ± 1080‰; Webster et al. 2013), whereas the Martian mantle (δD ≤ 275‰; Hallis et al. 2012; Usui et al. 2012) is close in composition to terrestrial reservoirs (δD −300 to 0‰; Lécuyer et al. 1998). Usui et al. (2015) suggested that Mars has a third hydrogen reservoir within hydrated crust or ground ice with an intermediate D/H ratio (δD 1000–2000‰). The hydrogen isotopic composition of iddingsite in Governador Valadares, Lafayette, Miller Range (MIL) 00346, Nakhla, and Yamato (Y)-000593 is in excess of terrestrial values. Nakhla, the only nakhlite fall, has yielded the highest δD of 1165‰ (Leshin et al. 1996; Hallis et al. 2012). Thus, water/OH in the iddingsite is interpreted to have equilibrated with Mars's atmosphere, but could equally have been derived from the hydrated crust/ice reservoir that was postulated by Usui et al. (2015). Iddingsite in Lafayette and Y-000593 has been dated to 633 ± 23 Ma (Borg and Drake [2005] and references therein), meaning that with regard to those two meteorites at least, the liquid water that was responsible for aqueous alteration cannot have been sourced from the same episode of igneous activity that formed their parent rocks.

Northwest Africa (NWA) 817 has relatively abundant iddingsite that formed by aqueous alteration on Mars (Gillet et al. 2002). The δD value of its iddingsite (−170 ± 14‰) has been interpreted to show that the water responsible for alteration was derived from the Martian mantle (Gillet et al. 2002; Meunier et al. 2012). Taken together, the hydrogen isotopic data therefore suggest that the nakhlite launch site experienced two episodes of aqueous alteration—one by crustal/atmospheric fluids (recorded by iddingsite in Governador Valadares, Lafayette, MIL 00346, Nakhla, and Y-000593) and the other by mantle-derived solutions (recorded by NWA 817 alteration products). Furthermore, given that NWA 817 iddingsite has not been radiometrically dated, it is possible the liquid

water was sourced from the same episode of igneous activity that formed the nakhlite lavas at 1.4–1.3 Ga (Meunier et al. 2012). Here we test the idea that the nakhlites were altered by multiple fluids from different sources by comparing the petrographic, mineralogical, chemical, and isotopic properties of iddingsite in NWA 817 with other members of the group.

MATERIALS AND METHODS

NWA 817 was found in Morocco in December 2000 as a single 104 g stone (Grossman and Zipfel 2001), and was first described in detail by Gillet et al. (2002) and Sautter et al. (2002). This study has used three pieces of a commercially obtained sample, hereafter referred to as N8-1, N8-2, and N8-3. None of these pieces has a fusion crust. N8-1 was used for petrographic, mineralogical, and chemical analysis, whereas N8-2 and N8-3 were used for deuterium/hydrogen (D/H) measurements by stepwise pyrolysis. After the D/H work, a polished block was made from N8-3 in order to identify those components that had lost water/hydroxyls during pyrolysis.

The polished blocks made from N8-1 and N8-3 were coated with carbon and backscattered electron (BSE) images were acquired using two field-emission gun scanning electron microscopes (FEG-SEM), a Zeiss Sigma and a FEI Quanta 200F, both operated at 20 kV and under high vacuum. X-ray maps and quantitative chemical analyses were acquired using the Zeiss equipped with Oxford Instruments INCA and AZtec microanalysis systems operating through a X-Max silicon-drift energy-dispersive X-ray (EDX) detector. Mapping was undertaken at 20 kV/1–5 nA, whereas the quantitative analyses were acquired at 20 kV/1 nA with a 60 s count time. X-ray spectra were calibrated using the following mineral standards: jadeite (Na, Al), periclase (Mg) olivine (Si), apatite (P), pyrite (S), orthoclase (K), wollastonite (Ca), rutile (Ti), rhodonite (Mn), almandine garnet (Fe), and Ni-metal (Ni). The "feature mapping" function of AZtec was used to locate barite in N8-1 by automatically searching for grains falling within a predefined contrast range in BSE images. By setting this contrast band to detect only the brightest pixels (i.e., grains with a high mean atomic number, Z), grains of barite could readily be located, and their size, shape, petrographic context, and chemical composition could be determined. For electron backscatter diffraction (EBSD) work, N8-1 was polished for 4 h using 0.01 μm colloidal silica in a NaOH suspension, then coated with 5 nm of carbon. EBSD and EDX maps were acquired simultaneously from a 250 × 200 μm area of mesostasis at Oxford Instruments Nano-analysis, High Wycombe, using a Hitachi SU-70 field-emission SEM equipped with an Oxford Instruments CMOS-based Symmetry EBSD detector and X-Max 80 mm^2 EDX detector. The SEM was operated at 15 kV/12 nA, and mapping was undertaken at a step size of 200 nm. The data were acquired using AZtec EDX-EBSD software v. 3.4., and the electron backscatter patterns (EBSP) were collected at resolutions of 156 × 128 pixels/EBSP to allow the acquisition of 247 patterns/s. The data were processed and interpreted using Oxford Instruments HKL Channel 5 software. Noise reduction using a single "wildspike" correction was followed by an iterative 6 point nearest neighbor zero solution correction, which is routine for this type of data (Watt et al. 2006; Forman et al. 2016, 2017). Grains were identified using the Channel 5 grain detection algorithm where a single grain is defined as <10° misorientation across adjacent pixels.

Electron-transparent samples for transmission electron microscopy (TEM) were extracted from N8-1 using a FEI DuoMill dual-beam focused ion beam (FIB) instrument. Milling employed a 30 kV Ga^+ ion beam at various currents following the protocol of Lee et al. (2003). The ~100 nm thick samples were studied initially by low-voltage scanning TEM (LV-STEM) imaging in the Quanta SEM (Lee and Smith 2006), then bright-field and high-resolution images, and selected area electron diffraction (SAED) patterns were acquired using a FEI T20 TEM operated at 200 kV. Subsequently, high-angle annular dark-field (HAADF) images and EDX analyses were obtained from the same foils using a JEOL ARM200F aberration-corrected TEM that was operated at 200 keV/~100 pA, giving a nominal spot size of <0.2 nm. The EDX analysis used a Bruker 60 mm^2 SDDEDX spectrometer, and spectra were quantified using proprietary software.

The D/H work on N8-2 and N8-3 used chips (77.5 and 108 mg, respectively) in preference to powders in order to minimize contamination by the terrestrial atmosphere. These samples were placed in an all-glass vacuum line and pumped down overnight. They were incrementally heated in a temperature-controlled induction heater to 200, 500, and 1050 °C (±5 °C). Samples were held at each designated temperature for a minimum of 15 min. The gases released were initially stored in a cold trap at −196 °C using a liquid nitrogen bath. This bath was then replaced by a mixture of dry ice and acetone at −78 °C, trapping water but releasing other gases. The yield of gas not trapped at −78 °C was measured using an Edwards PR10-C Pirani vacuum pressure gauge. The dry ice and acetone bath was then removed from the cold trap, which was gently heated, and the water was released. This water was reduced to hydrogen via exposure to chromium powder at 850 °C

(Donnelly et al. 2001). The hydrogen gas yield for each step was measured using the Pirani vacuum pressure gauge, and the hydrogen collected using a mercury topo pump. Hydrogen isotopes were measured using a VGI Optima mass spectrometer. In-run repeat analyses of water standards (international standards GISP, V-SMOW, and internal standard LT-STD) gave a reproducibility better than ± 2‰ for δ^2H.

RESULTS

Petrography and Mineralogy of NWA 817

The modal mineralogy of NWA 817, in vol%, is: 69% pyroxene, 10–15% olivine, 15–20% mesostasis, and 1% Fe-Ti oxide (Gillet et al. 2002; Sautter et al. 2002). Olivine grains in the sample studied are euhedral or subhedral single crystals (Fig. 2). They are zoned, with a measured core-to-rim compositional range of Fa_{57} to Fa_{85}, respectively, which is in good agreement with previous analyses (Sautter et al. 2002; Richter et al. 2016). Grain cores are compositionally uniform and with an oval outline (Fig. 2). Augite crystals are also zoned, with narrow Fs-rich rims (Fig. 1a). EBSD shows that the mesostasis is composed primarily of elongate laths of feldspar, many of which are twinned, and EBSP patterns acquired from these laths were indexed using an albite reference (Fig. 3). Other constituents include apatite, augite, cristobalite, olivine (including 5–10 μm size fayalite dendrites), and titanomagnetite grains containing ilmenite lamellae (Fig. 3). A few regions of the mesostasis produced EBSP with no Kikuchi bands, suggesting the presence of glass, a nanocrystalline phase, or an electron beam-sensitive material (Prior et al. 2009). Minerals within the mesostasis and the rims of the phenocrysts have been deformed (Fig. 3). The active slip systems that have accommodated deformation within the fayalite dendrites are [100] and [010], dominated by (010)[100] and (001)[100], which is consistent with A-Type and E-Type slip, respectively (Karato et al. 2008) (Fig. 3).

N8-1 is crosscut by 1–3 μm wide fractures, many of which contain calcite (Figs. 1b and 4a–c). These fractures are most common in augite, can also occur in olivine, but are rare in the mesostasis (Figs. 1b and 4b). Grains of barite, some Sr-rich, occur throughout N8-1, and the 7.1×10^4 μm^2 area that was analyzed by feature mapping contains 47 barite grains >300 nm in size. The hosts of these grains and their total size (expressed as μm^2) are as follows: olivine (14 grains/26 μm^2), augite (14 grains/17 μm^2), mesostasis (12 grains/38 μm^2), and fractures (7 grains/219 μm^2). Barite also occurs within veins of iddingsite outside of the mapped region (Fig. 5).

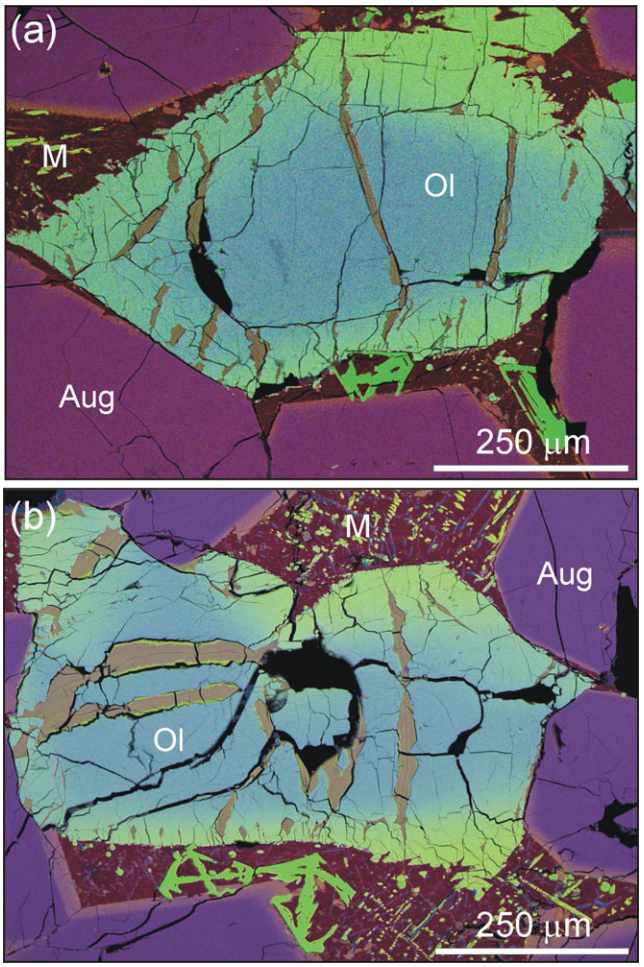

Fig. 2. Phenocrysts of olivine (Ol) in N8-1. The images have been made by overlaying X-ray maps on BSE images. The X-ray maps are a blend of three element maps: Si Kα (red), Mg Kα (blue), and Fe Kα (green). These color combinations render augite (Aug) grain cores purple, the narrow Fs-rich rims to augite grains pink, olivine grain cores blue, olivine grain rims light green, iddingsite brown, skeletal crystals of Fe-Ti oxide lime green, and the mesostasis (M) predominantly dark red. a) An olivine phenocryst that is zoned from a relatively Fa-poor core to a narrow Fa-rich rim and is crosscut by three iddingsite veins. The vein on the left-hand side follows the curved boundary between the core and rim. Shorter and discontinuous veins occur only in the Fa-rich grain rim. b) A zoned olivine phenocryst that contains relatively wide iddingsite veins in two orientations. The Fa-rich rim along the bottom edge of the grain contains many short and discontinuous iddingsite veins. (Color figure can be viewed at wileyonlinelibrary.com.)

Olivine-Hosted Iddingsite Veins

Vein Microstructure and Microstratigraphy

Iddingsite occurs as patches in the mesostasis and within grains of pyroxene (Gillet et al. 2002), but is most abundant as veins in olivine (Figs. 1a, 2, and 4a).

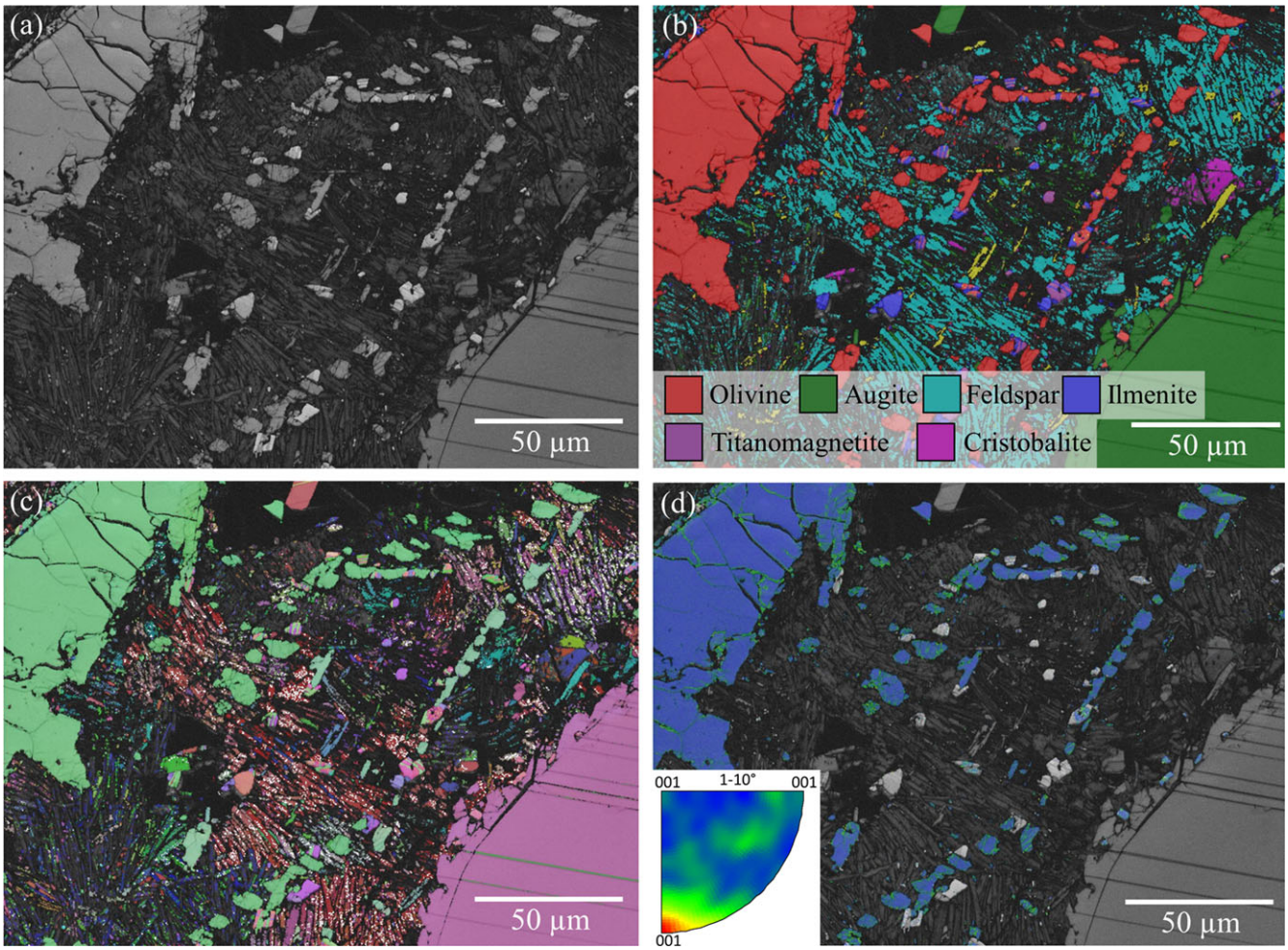

Fig. 3. EBSD images of a region of mesostasis in N8-1. a) EBSD band contrast map. The brighter regions have produced higher quality EBSPs. No EBSPs were detected within black areas. b) Band contrast map overlain with a phase map indicating the distribution of minerals within the mesostasis. c) Band contrast map overlain with a Euler map where colors represent different orientations relative to the plane of the section. Note the twinning in the feldspar laths that is identifiable by Euler color changes across a linear feature within a single lath (highlighted with thin white lines) or as variable band contrast within a single lath across a linear feature observable in (a). d) Band contrast map with the olivine crystals overlain with a local misorientation map. No misorientation in adjacent indexed pixels is colored blue and increasing degrees of misorientation in adjacent pixels are colored green to yellow through red for the maximum degree of misorientation. The inverse pole figure indicates the misorientation rotation axis that accommodates the deformation and is dominated by [100] slip, typical of A-Type slip systems (Karato et al. 2008). (Color figure can be viewed at wileyonlinelibrary.com.)

SEM point counting of four grains shows that they contain 5.7–20.0 vol% iddingsite (mean 11.6 vol%; 2024 points counted). The abundance of olivine in NWA 817 (10–15 vol%) means that iddingsite veins comprise ~1.2–1.7 vol% of the whole rock. These veins are red-orange in color when viewed in thin section using plane polarized transmitted light (Sautter et al. 2002), and have a lower Z than their host olivine. They are most abundant in the Fe-rich rims of olivine grains, where they are typically a few tens of micrometers in length by submicrometer in width, and have finely serrated walls (Fig. 2). Veins that crosscut olivine grain cores are up to 40 µm in width, frequently curved, and may have coarsely serrated walls (Figs. 4a and 5a). Almost all veins terminate abruptly at olivine grain margins, and so do not continue into adjacent augite grains or the mesostasis (Fig. 2).

Three components of the iddingsite can be recognized by differences in atomic number (Z) and location within the veins (1) low-Z axial bands; (2) mid-Z body of the vein; (3) high-Z rims (Fig. 5). The axial bands are ~1 µm in width, and straight or gently curving, regardless of the shapes of the vein walls (i.e., the axial bands do not zig-zag or pinch and swell in step with teeth and notches of the serrations) (Figs. 5a and 5b). Mid-Z iddingsite is the volumetrically

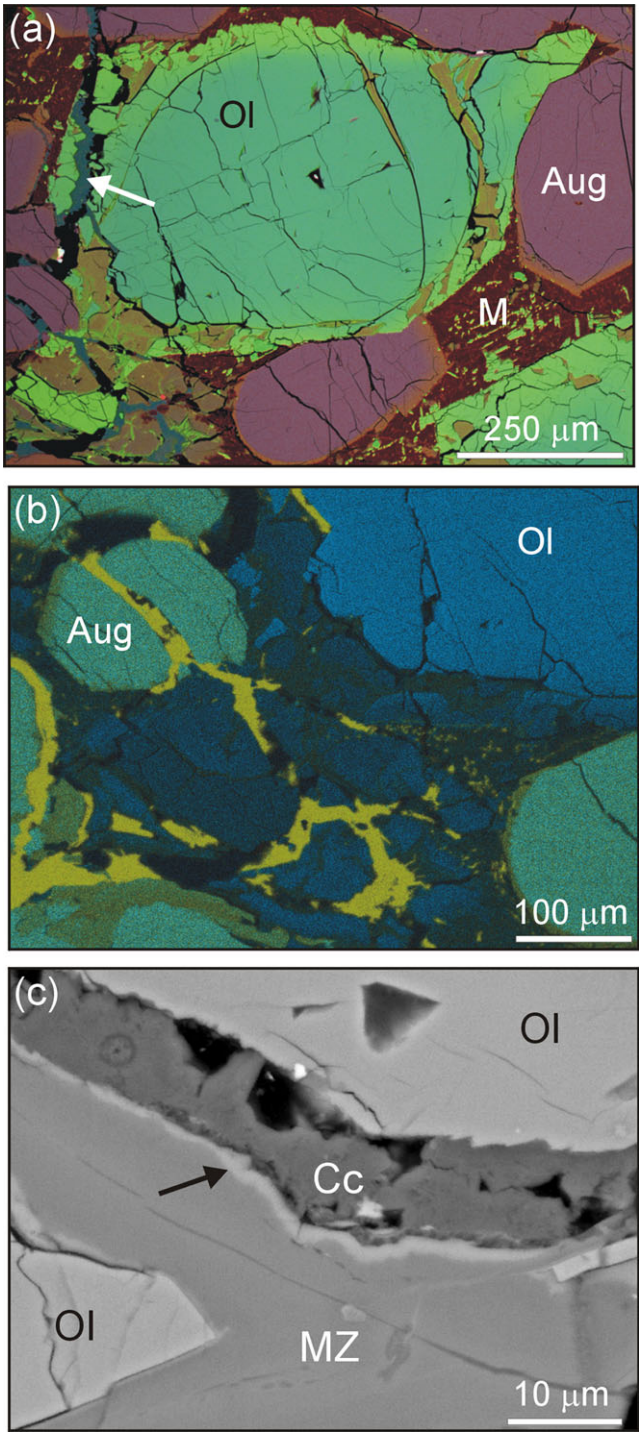

Fig. 4. An altered phenocryst of olivine (Ol) in N8-1. a) X-ray map overlain on a BSE image. The X-ray map has been made by blending three element maps: Si Kα (red), Mg Kα (blue), and Fe Kα (green). These color combinations render augite (Aug) grain cores purple, the narrow Fs-rich rims to augite grains dark orange, olivine grain cores light blue, olivine grain rims light green, iddingsite brown, calcite dark blue-green (indicated by white arrow), and the mesostasis (M) predominantly dark red. Iddingsite veins occur mainly in outer parts of the olivine grain core and in its rim. b) X-ray map of an area in the lower left hand corner of (a) that was made by blending maps of Mg Kα (blue) and Ca Kα (yellow). This element combination renders olivine mid blue to dark blue, augite turquoise, and the anastomosing veins of calcite yellow. c) BSE image of a vein of calcite (Cc) that occurs between mid-Z iddingsite (MZ) and olivine. High-Z iddingsite (light gray selvage indicated by a black arrow) occurs between mid-Z iddingsite and calcite, whereas the contact between olivine and mid-Z iddingsite in the lower left hand side of the image has very little high-Z iddingsite. (Color figure can be viewed at wileyonlinelibrary.com.)

dominant vein constituent, and is featureless in BSE images (Figs. 5a and 5b). High-Z iddingsite forms a 1–4 μm wide selvage along vein walls, and crosscuts the mid- and low-Z components as narrow veins (Fig. 5b). Selvages of high-Z iddingsite can occur where the mid-Z iddingsite is juxtaposed with veins of calcite (Fig. 4c), but high-Z iddingsite is also present in the absence of calcite. Fibers of high-Z iddingsite penetrate into olivine (Fig. 5c), and can also crosscut the axial bands to make a ladder-like structure (Fig. 5d). All three iddingsite components are crosscut by veins of calcite, and the high-Z iddingsite contains narrow veins of barite (these veins were too small and rare to have been identified by Feature mapping; Fig. 5c).

Iddingsite Chemical Composition and Mineralogy

The low- and mid-Z iddingsite is composed principally of Si, Mg, and Fe, and yields analytical totals of ~89 wt%; the remaining 11 wt% is likely comprised of water and other volatiles not measured by SEM-EDX (Table 1). The low-Z axial bands have a higher Mg/Fe ratio than mid-Z iddingsite (Table 1; Fig. 6). Both the low- and mid-Z iddingsite are featureless in bright-field TEM images, although the two components can be distinguished by subtle differences in their degree of electron scattering, which reflects contrasts in Z (Fig. 7a). High-resolution TEM shows that the axial bands contain crystals with a ~1 nm lattice spacing that are 3–4 layers thick (i.e., 3–4 nm) (Fig. 7b). Mid-Z iddingsite also contains crystals with a ~1 nm basal layer spacing, but which are smaller than those in the axial bands (i.e., 2–3 layers thick). SAED patterns acquired from the mid-Z iddingsite have continuous rings, which is consistent with the randomly oriented nanocrystals observed by high-resolution TEM.

High-Z iddingsite has greater concentrations of Ca, Mn, and Fe, and lower Si and Mg than the low- and mid-Z iddingsite, and its analytical totals are also lower (~86 wt%) (Table 1; Fig. 6). TEM images of a vein of high-Z iddingsite that crosscuts the two other

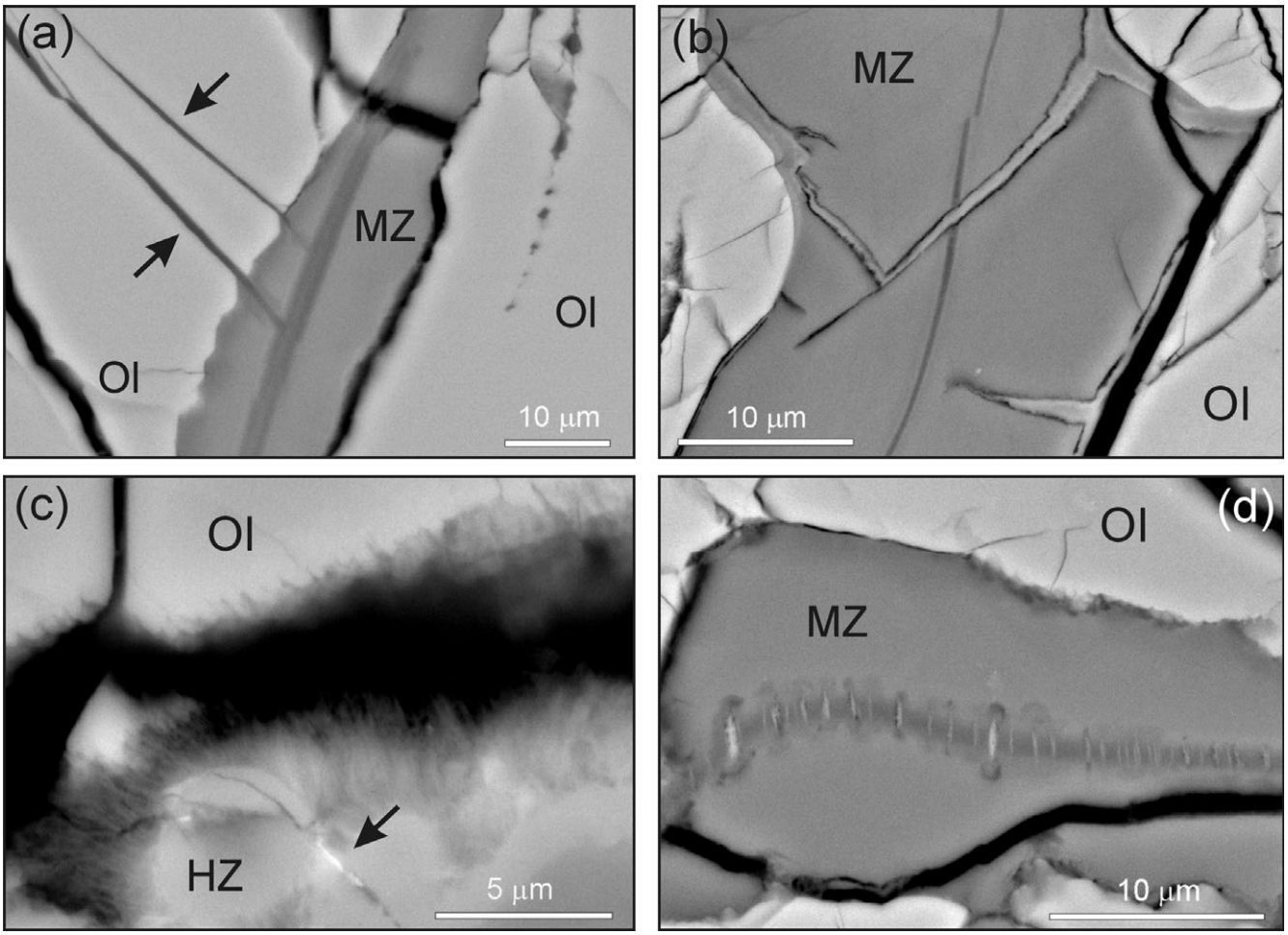

Fig. 5. BSE images of iddingsite veins within olivine (Ol) phenocrysts from N8-1. a) The vein in the center of the image has an axial band of low-Z iddingsite that is flanked by mid-Z iddingsite (MZ). A pair of narrow low-Z veins (arrowed) extend from the left-hand side of the axial band into olivine. b) A vein containing a low-Z axial band, mid-Z iddingsite (MZ), and high-Z iddingsite. The high-Z component occurs as a selvage between mid-Z iddingsite and olivine, and as veins that crosscut mid-Z iddingsite and the axial band. c) The interface between high-Z iddingsite (HZ) and the olivine vein wall, along which is a fracture (black). Fine fibers project from high-Z iddingsite across the fracture and into olivine. Barite (white) occurs within the high-Z iddingsite (arrowed). d) A vein that is dominated by mid-Z iddingsite (MZ) whose axial band (dark gray) is crosscut by needles of high-Z iddingsite that together make a ladder-like texture.

components shows that it comprises a central compact band that is rimmed by curved fibers. The interface between the curved fibers and the low- and mid-Z iddingsite is crenulated (Fig. 7c). The fibers have a basal layer spacing of 1 nm, and contain packets up to ~20 layers in thickness (Fig. 7d). The structural formula, $(Ca,K)_{0.6}(Al,Mg,Fe,Mn)_{4.6}[(Si,Al)_8O_{20}](OH)_4$, is consistent with the dioctahedral smectite nontronite (Table 1).

Iddingsite Hydrogen Isotopic Composition

N8-2 and N8-3 evolved almost identical amounts of water during stepped pyrolysis (0.45 and 0.47 wt%, respectively), and δD values are similar between the two samples (Table 2). SEM imaging of N8-3 shows that heating to 1050 °C has led to almost complete loss of calcite, and shrinkage and fracturing of the iddingsite veins. The mean atomic number of the low- and mid-Z iddingsite in the heated samples is similar to that of the olivine, and SEM-EDX analyses give totals that are close to 100 wt% (Table 3).

DISCUSSION

We have sought to answer the question of whether NWA 817 was altered under different physico-chemical conditions than the other nakhlites, by fluids of a different provenance (i.e., derived from the Martian mantle as opposed to the atmosphere/crust of Mars), and possibly also at a different time. We first explore

Table 1. Chemical composition of iddingsite in N8-1.

	SEM-EDX		TEM-EDX			
	Low- & mid-Z[a]	High-Z	Low-Z	Mid-Z	High-Z	High-Z fiber
SiO_2	42.49	25.40	47.1	48.40	30.0	48.0
Al_2O_3	0.36	0.84	1.2	0.6	0.7	11.6
Fe_2O_3	37.92	47.61	36.0	43.9	61.2	31.1
MnO	0.46	5.33	0.4	0.5	1.5	0.5
MgO	6.07	1.96	11.5	5.9	1.3	4.9
CaO	0.06	3.85	3.0	0.1	4.7	2.0
K_2O	0.50	0.13	0.8	0.5	0.7	1.9
Na_2O	0.35	0.18	bd	bd	bd	bd
SO_3	0.05	bd	bd	bd	bd	bd
Total	88.25	85.30	100.0	99.9	100.1	100.0
n	31	3	4	4	4	1
Cations per 22 oxygens						
Si	6.745	4.742	6.551	6.780	4.748	6.491
Al (tetrahedral)	1.255	3.258	1.449	1.220	3.252	1.509
	8.000	8.000	8.000	8.000	8.000	8.000
Al (octahedral)	−1.187	−3.073	−1.252	−1.121	−3.122	0.339
Fe^{3+}	4.526	6.682	3.764	4.623	7.281	3.161
Mn	0.062	0.843	0.047	0.059	0.201	0.057
Mg	1.437	0.545	2.385	1.232	0.307	0.988
	4.837	4.997	4.944	4.793	4.668	4.546
Ca	0.010	0.770	0.447	0.015	0.797	0.290
K	0.101	0.031	0.142	0.089	0.141	0.328
Na	0.108	0.065	–	–	–	–
S	0.018	0.000	–	–	–	–
	0.237	0.866	0.589	0.104	0.938	0.618
Total	25.910	26.860	26.860	25.690	26.273	25.709

[a]The low-Z axial bands were too narrow to individually chemically analyze by SEM-EDX, but were included in some of the analyses of mid-Z iddingsite.
bd = below the limits of detection.
Ti, Cr, and Ni were sought but not detected in all samples.

the processes and products of aqueous alteration of NWA 817, and compare results with work on the other nakhlites. We then evaluate the hydrogen isotopic data and conclude with a discussion of the implications of our findings for understanding the history of liquid water at the nakhlite launch site.

Environments of Aqueous Alteration of NWA 817

NWA 817 contains a suite of alteration products whose crosscutting relationships describe a relative chronology of water/rock interaction. Iddingsite formed first, and was followed by calcite (Fig. 4c). Barite occurs within high-Z iddingsite and so formed after all three iddingsite components (Fig. 5c), although the relative timing of barite and calcite precipitation could not be resolved. Calcite and barite are commonplace in hot desert ordinary chondrite finds where they are interpreted to be products of terrestrial weathering (Ash and Pillinger 1995; Barrat et al. 1998; Lee and Bland 2004; Al-Kathiri et al. 2005). As outer parts of Saharan meteorites (and, by extension, other hot desert meteorites) are often enriched in barium, it will have been sourced externally (Stelzner et al. 1999). The veins calcite and barite that occur in hot desert shergottite and nakhlite finds (Coulson et al. 2007; Tomkinson et al. 2015; Hallis et al. 2017), including NWA 817, are likewise interpreted to be terrestrial in origin. The association of calcite with augite in NWA 817 (Fig. 1b) implies that a proportion of the calcium could have been derived from the dissolution of clinopyroxene. In later sections, we discuss the implications of this hot desert weathering of NWA 817 for interpreting the hydrogen isotopic results.

Formation of NWA 817 Iddingsite

The microstratigraphy of the olivine-hosted iddingsite veins shows that there are three components formed in the order of low-Z, mid-Z, and then high-Z.

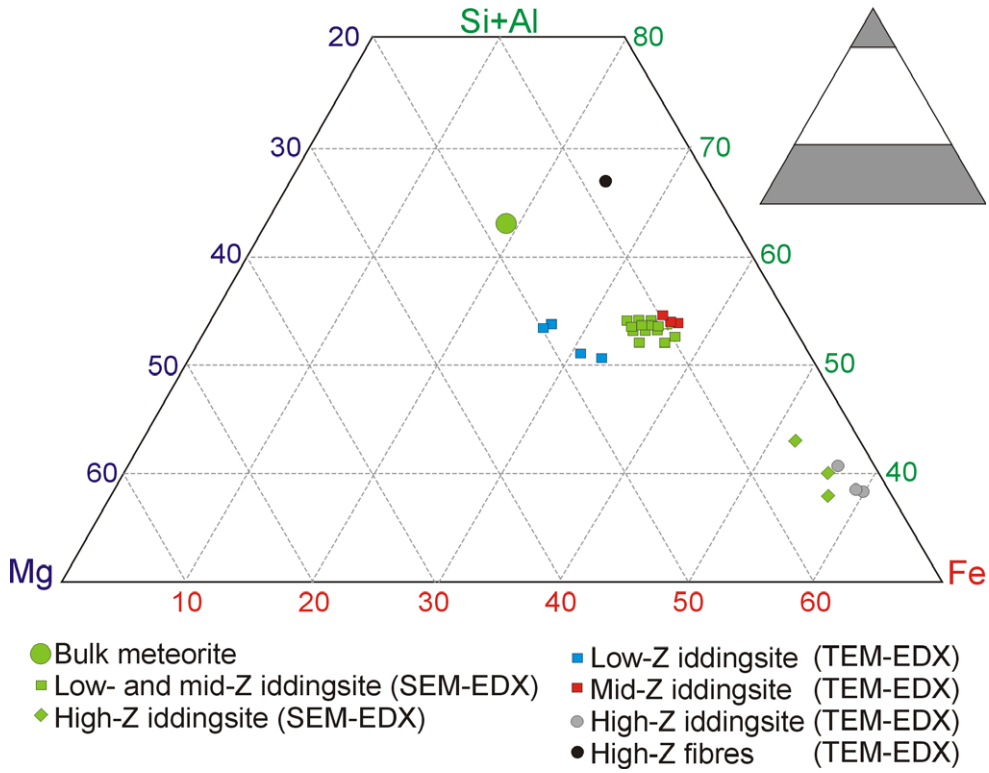

Fig. 6. The chemical composition of iddingsite in N8-1 (expressed as atom%, this study). Also plotted is the bulk composition of the meteorite from Sautter et al. (2002). (Color figure can be viewed at wileyonlinelibrary.com.)

The low-Z axial band is interpreted to have filled hairline fractures (e.g., Figs. 5a and 5b). The walls of these narrow veins were then replaced to make the mid-Z iddingsite, during which time serrations developed in response to a crystallographic control on the trajectory of the replacement front (Lee et al. 2013). The higher abundance of iddingsite veins in the rims than cores of olivine grains probably reflects the greater susceptibility of Fa-rich olivine to aqueous alteration (e.g., Wogelius and Walther 1992). A control on iddingsite vein formation by olivine chemistry can also account for curved veins, whose intragranular distribution is controlled by the shape of the boundary between the core and rim of zoned phenocrysts (Fig. 4a).

The compositional evolution of iddingsite is characterized by depletion in Mg from low-Z to mid-Z iddingsite followed by decreases in Mg, Al, and Si in the high-Z iddingsite, with complementary enrichment with respect to Ca, Mn, and Fe (Fig. 6, Table 1). One of the hosts of these elements is smectite, and our identification of this clay mineral agrees with Gillet et al. (2002), who described ferromagnesian smectite in NWA 817 using X-ray diffraction and TEM. However, smectite cannot be the sole constituent of low- and mid-Z iddingsite because the veins have considerably lower concentrations of Al and/or Si, and higher Fe, than terrestrial Fe-Mg smectites such as nontronite, saponite, and montmorillonite (Deer et al. 1992). Structural formulae highlight the lack of octahedral Al (Table 1). The low- and mid-Z iddingsite is similar in chemical composition to iddingsite that has replaced olivine in terrestrial metagabbros (Kendrick and Jamieson 2016; Table 3). Raman spectroscopy showed that this terrestrial iddingsite contains amorphous hydrated silica and goethite; smectite was not recorded by Kendrick and Jamieson (2016), but this is perhaps unsurprising given the difficulty in identifying nanoscale crystals of such minerals by Raman spectroscopy. We therefore suggest that the low- and mid-Z iddingsite in NWA 817 contains an Al-poor and Mg-rich smectite, probably saponite, intergrown with Fe-oxyhydroxide (goethite/ferrihydrite) and some silica. The temperature range over which water is evolved from NWA 817 during pyrolysis (i.e., ~89% at <500 °C; Table 2) is also consistent with such a mineralogy (Archer et al. 2014; Garenne et al. 2014).

The high-Z component has replaced earlier iddingsite, and its occurrence as a selvage along vein walls shows that aqueous solutions gained access to olivine grain interiors via these intragranular boundaries. The veins of high-Z iddingsite comprise a

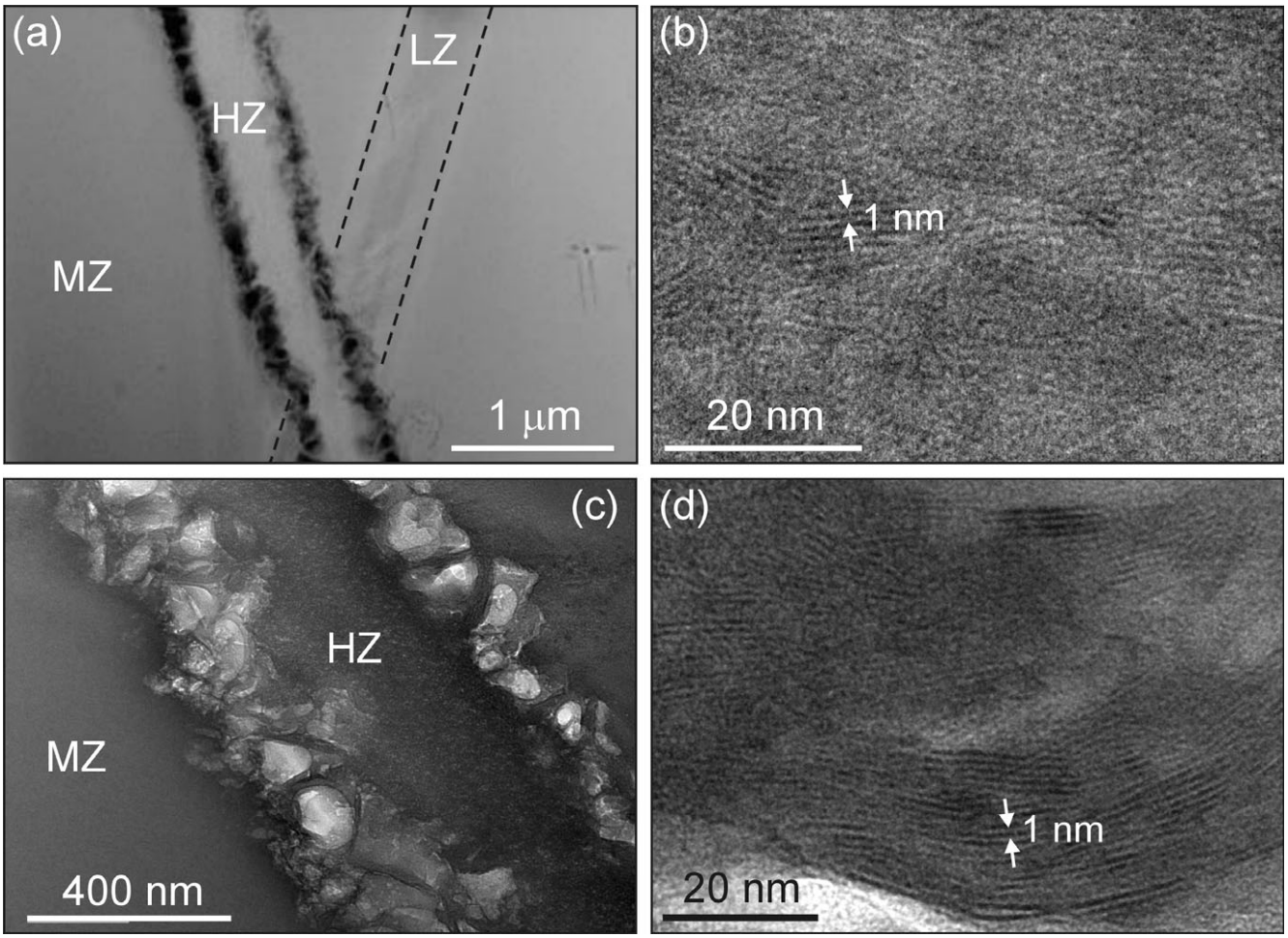

Fig. 7. TEM images of iddingsite in N8-1. a) HAADF STEM image of all three iddingsite components. A vein of high-Z iddingsite (HZ) crosscuts mid-Z (MZ) iddingsite and the low-Z axial band (LZ). b) High-resolution image of the low-Z iddingsite. Many small crystals are present, whose lattice fringes have a ~1 nm spacing. c) Bright-field image of high-Z iddingsite crosscutting mid-Z iddingsite. Between the two iddingsite components are curved smectite crystals and pores (white). d) High-resolution image of a smectite crystal between mid- and high-Z iddingsite. The lattice fringes have a ~1 nm spacing.

Table 2. Stepwise pyrolysis results from N8-2 and N8-3.

Sample	Step (°C)	Yield mmols/mg	H_2O (wt%)	δD (‰, V-SMOW)
N8-2[a]	200	0.04	0.07	−31.0
	500	0.18	0.32	−29.6
	1050	0.03	0.05	−23.8
Total		0.25	0.45	
N8-3[b]	200	0.10	0.20	28.7
	500	0.12	0.22	−103.1
	1050	0.03	0.05	−90.0
Total		0.25	0.47	

[a]Sample mass 77.5 mg.
[b]Sample mass 108 mg.

compact core lined by nontronite fibers. The core is rich in Fe and Si (~48 wt% Fe_2O_3, ~25 wt% SiO_2) but its chemical composition does not match that of a single stoichiometric mineral. We suggest therefore that the core is composed of ferrihydrite or goethite (which have 85 and 90 wt% Fe_2O_3, respectively) with Si absorbed on crystal surfaces. Fe-oxyhydroxides can have up to 19 wt% SiO_2 as an absorbed component (Childs 1992; Andersen et al. 2009). Some of the silica detected in the high-Z core could also be present as inclusions of low- and mid-Z iddingsite, or unaltered olivine. As discussed below, the properties of low- and mid-Z iddingsite are consistent with a Martian origin, which was originally proposed by Gillet et al. (2002). As it crosscuts the two earlier components, high-Z iddingsite clearly formed during a later phase of water/rock interaction which could have been hot desert weathering given that Fe-oxyhydroxides are abundant in meteorites recovered from northwest Africa (Lee and Bland 2004).

Table 3. Chemical composition of iddingsite.

	NWA 817 low-and mid-Z iddingsite		
	N8-3[a]	N8-1[b]	Terrestrial iddingsite[c]
SiO_2	45.89	42.49	41.31
TiO_2	0.01	bd	0.01
Al_2O_3	0.78	0.36	0.10
Cr_2O_3	–	bd	0.01
Fe_2O_3	43.92	37.92	41.69
MnO	0.60	0.46	0.49
MgO	6.01	6.07	5.38
CaO	0.69	0.06	0.53
K_2O	1.28	0.50	0.07
Na_2O	1.16	0.35	0.03
SO_3	0.09	0.05	–
Total	100.43	88.25	89.62
n	20	31	33

Analyses of NWA 817 by SEM-EDX.
[a]Analyzed after stepwise pyrolysis to 1050 °C (so water and other volatile phases would have be removed). Expressing Fe as FeO reduces the total to 96.01 wt%.
[b]Analyses of unheated sample N8-1 (from Table 1, column 1).
[c]Sample G86-12 of Kendrick and Jamieson (2016).
In all analyses, Fe is expressed as Fe_2O_3 to aid comparison.
– = not measured; bd = below detection limits.

Comparison of Alteration Products in NWA 817 with Other Nakhlites

From this understanding of the chemical composition and mineralogy of NWA 817 iddingsite, we now compare it with iddingsite from the other nakhlites in order to help answer the question of whether these meteorites were altered in the same aqueous system.

Iddingsite is most common within nakhlite olivine grains, which reflects the susceptibility of this mineral to low temperature aqueous alteration (Leshin and Vicenzi 2006). The microstratigraphy of the olivine-hosted veins is similar between NWA 817, Lafayette, and Nakhla. In all three meteorites, the veins possess an axial band that has a lower Z than the rest of the vein, and this internal structure is consistent with an origin by centripetal replacement starting from a hairline fracture (Velbel 2012; Tomkinson et al. 2013; Lee and Lindgren 2016; Lee et al. 2013, 2015a, 2015b). The abundances of iddingsite can be quantified by SEM (i.e., by point counting or image analysis of thin sections), or inferred from the volume of water evolved during stepped pyrolysis. Both measures reveal considerable differences between the nakhlites, with NWA 817 containing the most iddingsite and evolving the most water (Table 4). All of the meteorites listed in Table 4 evolved more water than would be expected from the volume of olivine-hosted iddingsite that has been recorded by SEM. For example, assuming that iddingsite contains 12 wt% water (Table 1), NWA 817 should have evolved only 0.14–0.21 wt% water from its 1.16–1.74 vol% of iddingsite. Some of the discrepancy with measured values (i.e., 0.45–0.47 wt% water; Table 2) can be accounted for by absorbed terrestrial water, which is released at low temperatures, and in the 200 °C step, NWA 817 evolved 0.07–0.20 wt%. Nonetheless, in order to account for all of the water that was evolved from NWA 817, some iddingsite or other water/OH-bearing minerals must be present in parts of the meteorite other than in olivine grains (i.e., augite or mesostasis), which is consistent with petrographic observations by Gillet et al. (2002). One reason why NWA 817 contains more iddingsite than the other three meteorites listed in Table 4 is likely to be the Fa-rich composition of its olivine, which will make it particularly susceptible to aqueous alteration.

Previous TEM studies have shown that the principal constituents of nakhlite iddingsite are smectite and Fe-oxyhydroxide/Fe-oxide (see table 3 in Lee et al. 2015a). As NWA 817 iddingsite is mineralogically comparable to the other nakhlites, all members of this meteorite group are likely to have been altered under similar physico-chemical conditions. Treiman et al. (1993) and Treiman and Lindstrom (1997) concluded that the smectite-ferrihydrite–dominated iddingsite in Lafayette was formed from fluids that had acquired solutes by dissolution of mesostasis glass and olivine over a brief period of time, at low temperatures (<100 °C) and low water/rock ratios. The presence of smectite suggests a moderate to alkaline pH (Mustard et al. 2008).

In order to compare the chemical composition of iddingsite between different nakhlites, a compilation was made of published SEM-EDX/electron probe analyses (Fig. 8). Significant numbers of analyses (i.e., >12) are available for only four of the nakhlites: Lafayette, Nakhla, NWA 817, and MIL 00346 (by contrast between two and four analyses are available for each of NWA 998, Governador Valadares, Y-000593, and Y-000749). The data for Lafayette, Nakhla, NWA 817, and MIL 00346 show that iddingsite in each meteorite has a narrow range in Mg concentrations, but a considerable spread in Al+Si and Fe values (Table 5; Fig. 8). Magnesium concentrations increase in the order of MIL 03346–NWA 817–Nakhla–Lafayette (Table 5). This variation in Al+Si and Fe at a fairly constant Mg could be accounted for by differences between analysis points in the relative proportions of smectite/silica and Fe-oxyhydroxide/Fe-oxide.

Martian Versus Terrestrial Sources of Aqueous Solutions

The similarities between nakhlites in the chemical composition and mineralogy of their iddingsite imply

Table 4. The abundance of iddingsite in four nakhlites and their water content.

Meteorite	Olivine (vol%)	Olivine-hosted iddingsite (vol%)	Whole rock iddingsite (vol%)	Whole rock water (wt%)
NWA 817	10–15[a,b]	11.6[c]	1.16–1.74	0.45–0.47[c]
Lafayette	14.5[d]	9.5–10.0[e,f]	1.38–1.45	0.373–0.387[g,h]
Nakhla	11.0[d]	2.5–5.0[e,f,i]	0.28–0.55	0.108–0.126[g,h]
Governador Valadares	10.1[d]	2.5–3.0[e,f]	0.25–0.30	0.11[g]

The abundance of iddingsite in the whole rock has been estimated by multiplying the volume of iddingsite within olivine grains by the volume of olivine in the rock.
Iddingsite within the mesostasis and pyroxene grains is not included.
[a]Gillet et al. (2002).
[b]Sautter et al. (2002).
[c]The present study: iddingsite abundance from N8-1 and water contents from N8-2 and N8-3.
[d]Corrigan et al. (2015).
[e]Changela and Bridges (2011).
[f]Hicks et al. (2014).
[g]Leshin et al. (1996).
[h]Karlsson et al. (1992).
[i]Lee et al. (2013).

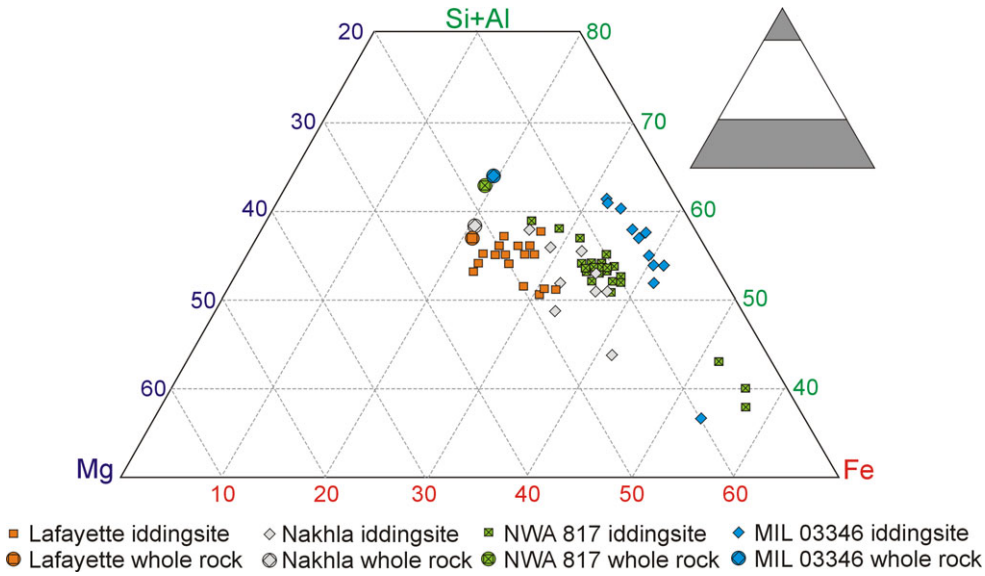

Fig. 8. Bulk chemical compositions of four of the nakhlites and their iddingsite (atom%). The bulk rock data were sourced as follows: Lafayette (Boctor et al. 1976), Nakhla (mean of analyses in McCarthy et al. 1974; Dreibus et al. 1982; Anand et al. 2005), NWA 817 (Sautter et al. 2002), and MIL 03346 (mean of analyses in Anand et al. 2005; Day et al. 2006). The iddingsite analyses plotted have been obtained by SEM-EDX or electron probe and so will average the compositions of different intergrown generations (e.g., NWA 817 low- and mid-Z iddingsite). The iddingsite data were sourced as follows: Lafayette (Bunch and Reid 1975; Boctor et al. 1976; Treiman et al. 1993; Bridges and Grady 2000; Vicenzi et al. 2002; Kuebler et al. 2004; Changela and Bridges 2011; Tomkinson et al. 2013; Hicks et al. 2014), Nakhla (Bunch and Reid 1975; Gooding et al. 1991; Changela and Bridges 2011; Hallis et al. 2012, 2014; Hicks et al. 2014; Lee et al. 2013, 2015a; Lee and Chatzitheodoridis 2016; Goodrich et al. 2013), NWA 817 (Gillet et al. 2002; Sautter et al. 2002; Hicks et al. 2014; the present study), and MIL 03346 (Day et al. 2006; Sautter et al. 2006; Imae and Ikeda 2007; Hallis and Taylor 2011; Kuebler 2013; Hallis et al. 2014; Hicks et al. 2014). (Color figure can be viewed at wileyonlinelibrary.com.)

that they were altered under comparable conditions (e.g., Eh, pH), but it does not necessarily follow that fluids came from the same reservoir. Here we explore whether the hydrogen isotopic data are consistent with a single source or multiple sources of the aqueous solutions, and whether the fluids were solely Martian or both Martian and terrestrial.

The hydrogen isotopic composition of NWA 817 iddingsite shows similarities but also some differences to the other nakhlites (Fig. 9). All of the analyzed

Table 5. The chemical composition of iddingsite and its host rock.

	Mean Mg/(Al+Si+Fe)		Mean MgO (wt%)		
Nakhlite	Iddingsite	Bulk rock	Iddingsite	Bulk rock	$^{40}Ar/^{39}Ar$ age ± 2σ (Ma)[a]
Lafayette	0.241 (0.033)	0.282	12.01 (2.22)	12.90	1321.7 ± 9.6
Nakhla	0.153 (0.040)	0.259	7.10 (1.75)	11.91	1382.5 ± 6.6
NWA 817	0.122 (0.025)	0.216	5.83 (1.24)	10.31	
MIL 03364	0.065 (0.014)	0.198	3.26 (0.78)	9.30	1390.9 ± 8.9

[a]Ages from Cohen et al. (2017). NWA 817 was not analyzed by them.

Iddingsite mean compositions are from the following number of analyses: Lafayette 20, Nakhla 12, NWA 817 41, MIL 03346 16. Values in parentheses are standard deviations.

Bulk rock mean compositions are from the following number of analyses: Lafayette 1, Nakhla 3, NWA 817 1, MIL 03346 2. Standard deviations not quoted owing to the small number of analyses.

The sources of all analyses are listed in the caption of Fig. 8.

meteorites yield some low δD values, which reflect terrestrial contamination (Leshin et al. 1996; Hallis et al. 2012). However, NWA 817 differs from the other nakhlites in that its δD values do not exceed 30‰ (Table 2; Fig. 9). Gillet et al. (2002) interpreted the unusually low δD values of NWA 817 to indicate that its iddingsite had formed from fluids derived from the Martian mantle. They discounted the possibility that the hydrogen isotopic system had been disturbed by terrestrial alteration because they found little evidence for hot desert weathering. However, the samples analyzed for the present study have been moderately weathered, producing calcite, barite, and possibly also the high-Z iddingsite. The presence of calcite along olivine vein walls (Fig. 4c) is clear evidence that terrestrial water had been in contact with iddingsite. As hydrogen is a very light and mobile atom, the hydrogen isotopic system is vulnerable to alteration, and indeed previous work has shown that terrestrial weathering can significantly change the hydrogen isotopic composition of nakhlite iddingsite. For example, Hallis et al. (2012) obtained very different δD values from iddingsite in the paired Antarctic nakhlites MIL 03346 and MIL 090030 (Fig. 9), presumably reflecting contrasting intensities of weathering. Even in Nakhla, which fell in 1911, individual analysis points range in δD from −117 to 1165‰ due to spatially variable terrestrial contamination (Hallis et al. 2012). Exchange of hydrogen isotopes between iddingsite and terrestrial water would have been facilitated by the high temperatures that NWA 817 is likely to have experienced during hot desert weathering; temperatures beneath the surfaces of low albedo rocks such as basalt in hot deserts can reach ~70 °C (Warke and Smith 1998).

This evidence for terrestrial fluids having been in contact with NWA 817 iddingsite means that the hydrogen isotopic data cannot be used with confidence to constrain the source of water that was responsible for

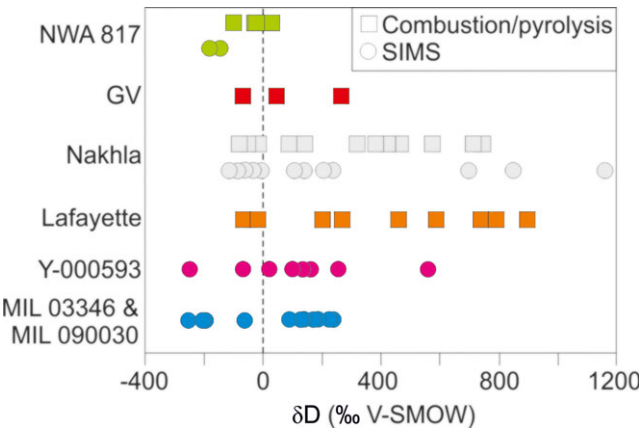

Fig. 9. Hydrogen isotopic composition of iddingsite in the nakhlites. The secondary ion mass spectrometry (SIMS) data are from Gillet et al. (2002) (NWA 817) and Hallis et al. (2012) (Y-000593, Nakhla, and the paired meteorites MIL 03346 and MIL 090030). The stepwise combustion/pyrolysis data are from the present study (NWA 817, Table 2) and Leshin et al. (1996) (Lafayette, Nakhla, Governador Valadares [GV]). δD values of all of the temperature steps are plotted. (Color figure can be viewed at wileyonlinelibrary.com.)

Martian aqueous alteration. While it remains possible that the low δD values reflect fluids derived from the Martian mantle, it is also conceivable that prior to its fall to Earth NWA 817 iddingsite had δD values of >1000‰, which were then lowered to <30‰ by hot desert weathering. Our EBSD results from the mesostasis give some weight to the argument that NWA 817 was not altered by aqueous fluids with a mantle composition derived from the igneous activity that formed the NWA 817 parent lava. Olivine slip systems are sensitive to temperature, pressure, strain rate, and water content (Karato et al. 2008). The dominant A-type slip system observed in the fayalite dendrites (Fig. 3) would have formed by rapid crystallization of the mesostasis during cooling under very dry conditions and at high temperatures >1000 °C (Carter and

Ave'Lallemant 1970; Jung and Karato 2001; Karato et al. 2008). While this evidence argues against aqueous alteration being linked to the phase of volcanic activity that formed NWA 817, it does not preclude the possibility that fluids could have been sourced from later magmatism at the same location. However, McCubbin et al. (2013) calculated that the nakhlite and chassignite magmatic fluids contained a minimum of 1.36 wt% Cl (within the Si-rich evolved melt that crystallized to form the intercumulus glass of MIL 03346). Therefore, if NWA 817 iddingsite did form from magmatic fluids, this Cl enrichment should be evident within its chemical composition. The absence of detectable Cl within NWA 817 iddingsite (Table 1) thus argues against a magmatic origin for this alteration product.

Implications for Understanding Aqueous Alteration at the Nakhlite Launch Site

The simplest interpretation of the mineralogical, chemical, and isotopic results obtained from NWA 817 is that it was altered on Mars, at the same time as the other nakhlites, and by D-rich solutions that were sourced from the Martian crust or atmosphere. The water was probably stored in permafrost, which could have melted in response to heating by a nearby impact or volcanic activity (Borg and Drake 2005). Volcanic heating is favored here because the low shock stage of the nakhlites (Fritz et al. 2005) is inconsistent with them having undergone two impacts (i.e., one to drive aqueous alteration at 633 Ma, and the other to eject the nakhlites from Mars). The crustal/atmospheric hydrogen isotopic signature was then overprinted by hot desert weathering. The low- and mid-Z iddingsite are interpreted to have formed on Mars, whereas the high-Z component could equally be terrestrial in origin.

Differences in $^{40}Ar/^{39}Ar$ ages between nakhlites can be used to reconstruct the stratigraphy of the nakhlite launch site by assuming that eruption age corresponds to stratigraphic position (i.e., the youngest nakhlite, Lafayette, samples the flow that was closest to the Martian surface; Cohen et al. 2017). The correspondence between the mean MgO value of iddingsite and the eruption age of its host meteorite (Table 5; Fig. 10) could therefore suggest that fluids evolved in chemical composition as they moved through the lava pile. The sense of compositional change could have been a decrease in Mg as the fluids flowed from shallower to deeper levels, or an increase in Mg as the water moved from deeper to shallower levels. Empirical support for the shallower-to-deeper scenario comes from the compositional evolution of NWA 817 iddingsite. The MgO values of the three generations (i.e., low-Z, mid-Z, high-Z) are 11.5 wt%, 5.9 wt%, and 1.3 wt%, respectively. Thus, Lafayette iddingsite is compositionally similar to NWA 817 low-Z iddingsite, suggesting that the Lafayette parent lava flow was altered by "primitive" near-surface fluids. MIL 03346 iddingsite is compositionally similar to NWA 817 mid-Z iddingsite, implying that the MIL 03346 parent lava flow interacted with more "evolved" and deeper fluids. A caveat to this model is that the $^{40}Ar/^{39}Ar$ age of the nakhlite NWA 5790 implies that it was in the middle of the lava pile (Cohen et al. 2017), yet in contrast to the overlying and underlying meteorites has little evidence for aqueous alteration (Tomkinson et al. 2015). Although this discrepancy could argue against the model of gravity-driven fluid flow, inhomogeneities in porosity and permeability of the lavas could readily explain why some meteorites escaped Martian aqueous alteration.

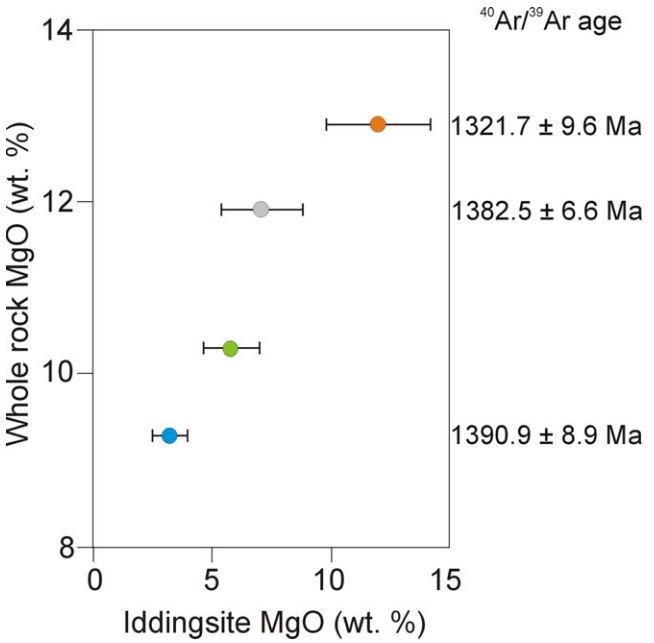

Fig. 10. The chemical composition of iddingsite plotted against that of its host meteorite. From the top of the graph downwards the meteorites are Lafayette (orange), Nakhla (gray), NWA 817 (green), and MIL 03346 (blue). Values are listed in Table 5. The eruption ages of three of the meteorites as determined by Cohen et al. (2017) are also shown. The position of NWA 817 in this plot comes from its whole rock and iddingsite chemical composition, and does not necessarily mean that its eruption age is between 1385.5 ± 6.6 and 1390.9 ± 8.9 Ma. (Color figure can be viewed at wileyonlinelibrary.com.)

Another interpretation of differences between meteorites in iddingsite MgO values is that they are controlled by the chemical composition of their host rock. Iddingsite and bulk rock compositions correlate well in Nakhla, NWA 817, Lafayette, and MIL 03346

(Fig. 10). Such a control on fluid compositions would suggest that water/rock ratios were very low (i.e., the chemistry of the system was rock-dominated). The nakhlites have a present-day water/rock ratio of 0.001–0.005 by weight, but this value is a minimum for conditions during aqueous alteration because only a small proportion of the water that moved through the rock is likely to have been retained by its alteration products. As the bulk MgO values for three of the meteorites under consideration decrease with increasing age, and so probably also with depth beneath the surface of Mars (Table 5; Fig. 10), a control on iddingsite chemistry by host rock composition can also explain the relationship between iddingsite chemistry and stratigraphic position. The two possible explanations for iddingsite chemistry in Fig. 10, down-flow compositional gradients and low water/rock ratios, cannot be distinguished using available information, but can be tested by obtaining more analyses of iddingsite from the other nakhlites that were dated by Cohen et al. (2017) (e.g., Y-00593 and Y-00749). It is also important to note that the correlation between whole rock MgO values and stratigraphic position that is implied by Fig. 10 does not hold when all six of the nakhlites dated by Cohen et al. (2017) are considered (i.e., there is no suggestion that the whole stack of lava flows shows a progressive enrichment in Mg over time). Thus, the relative position of NWA 817 in the nakhlite lava pile should ideally be confirmed by high precision chronology.

CONCLUSIONS

This study has sought to answer the question of whether NWA 817 was altered in the same aqueous system as the other nakhlites. The principal findings are as follows.

1. NWA 817 contains more iddingsite than any other nakhlite, thus testifying to a relatively high intensity of aqueous alteration on Mars. Even if the high-Z iddingsite is terrestrial in origin, it is insufficiently abundant to change this conclusion. The relatively high degree of aqueous alteration of NWA 817 could be explained by the unusually Fe-rich composition of its olivine grains, making them highly reactive in the presence of Martian groundwater.
2. In common with the other nakhlites, NWA 817 iddingsite occurs mainly as veins within olivine grains, and is composed of nanocrystalline smectite and a Fe-rich phase that is most likely to be Fe-oxyhydroxide. These petrographic and mineralogical similarities between iddingsite in the different meteorites suggest that the nakhlites were aqueously altered under comparable physico-chemical conditions.
3. NWA 817 iddingsite has lower δD values than any other nakhlite. However, as this meteorite has been terrestrially weathered to form calcite, barite, and possibly also high-Z iddingsite, the hydrogen isotopic data cannot be used with confidence to constrain the provenance of Martian aqueous solutions.
4. The nature of deformation of olivine crystals in the mesostasis of NWA 817 suggests that the rock was emplaced dry so that aqueous alteration is unlikely to have been linked to igneous activity associated with eruption of its parent lava flow. The possibility of alteration by later generations of magmatic fluids cannot be discounted, although the absence of detectable Cl within NWA 817 iddingsite argues against such a scenario.
5. The correspondence between the chemical composition of iddingsite and the stratigraphic position of its host rock could be interpreted to indicate that the aqueous solutions were sourced from close to the surface of Mars and evolved chemically down-flow. Alternatively, this relationship may reflect a control on the chemistry of iddingsite by the composition of its host rock in a system with very low water/rock ratios.
6. NWA 817 was probably aqueously altered along with the other nakhlites at $\sim$633 Ma and by water derived from crustal or atmospheric reservoirs.

Acknowledgments—We thank Peter Chung, Billy Smith, Colin How, and Sam McFadzean for help with the SEM, FIB, and TEM work, and Alison MacDonald for assistance with the hydrogen isotope analyses. Author contributions: M.R.L., B.E.C., L.D., D.F.M. designed the research project; M.R.L., B.E.C., L.D., S.G., P.T., A.B. undertook analyses; M.R.L., B.E.C., L.D., S.G., L.J.H., D.F.M., A.B. contributed to writing and editing of the paper; M.R.L., D.F.M. acquired funding. The manuscript benefitted considerably from helpful reviews by Agata Krzesińska and Michael Velbel. This work was funded by the Science and Technology Facilities Council through grants ST/N000846/1 and ST/H002960/1.

Editorial Handling—Dr. Josep M. Trigo-Rodríguez

REFERENCES

Al-Kathiri A., Hofmann B. A., Jull A. J. T., and Gnos E. 2005. Weathering of meteorites from Oman: Correlation of chemical and mineralogical weathering proxies with C-14 terrestrial ages and the influence of soil chemistry. *Meteoritics & Planetary Science* 40:1215–1239.

Anand M., Williams C. T., Russell S. S., Jones G., James S., and Grady M. M. 2005. Petrology and geochemistry of nakhlite MIL 03346: A new Martian meteorite from Antarctica (abstract #1639). 36th Lunar and Planetary Science Conference. CD-ROM.

Andersen J. C. Ø., Rollinson G. K., Snook B., Herrington R., and Fairhurst R. J. 2009. Use of QEMSCAN® for the characterization of Ni-rich and Ni-poor goethite in laterite ores. *Minerals Engineering* 22:1119–1129.

Archer P. D., Franz H. B., Sutter B., Arevalo R. D., Coll P., Eigenbrode J. L., Glavin D. P., Jones J. J., Leshin L. A., Mahaffy P. R., McAdam A. C., McKay C. P., Ming D. W., Morris R. V., Navarro-González R., Niles P. B., Pavlov A., Squyres S. W., Stern J. C., Steele A., and Wray J. J. 2014. Abundances and implications of volatile-bearing species from evolved gas analysis of the Rocknest aeolian deposit, Gale Crater, Mars. *Journal of Geophysical Research Planets* 119:237–254.

Ash R. D. and Pillinger C. T. 1995. Carbon, nitrogen and hydrogen in Saharan chondrites—The importance of weathering. *Meteoritics* 30:85–92.

Ashworth J. R. and Hutchison R. 1975. Water in non-carbonaceous stony meteorites. *Nature* 256:714–715.

Barrat J. A., Gillet P., Lecuyer C., Sheppard S. M. F., and Lesourd M. 1998. Formation of carbonates in the Tatahouine meteorite. *Science* 280:412–414.

Boctor N. Z., Meyer H. O. A., and Kellerud G. 1976. Lafayette meteorite: Petrology and opaque mineralogy. *Earth and Planetary Science Letters* 32:69–76.

Bogard D. D. and Johnson P. 1983. Martian gases in an Antarctic meteorite. *Science* 221:651–654.

Borg L. and Drake M. J. 2005. A review of meteorite evidence for the timing of magmatism and of surface or near-surface liquid water on Mars. *Journal of Geophysical Research* 110:E12S03.

Bridges J. C. and Grady M. M. 2000. Evaporite mineral assemblages in the nakhlite (Martian) meteorites. *Earth and Planetary Science Letters* 176:267–279.

Bunch T. E. and Reid A. M. 1975. The nakhlites Part 1: Petrography and mineral chemistry. *Meteoritics* 10:303–315.

Carter N. L. and Ave'Lallemant H. H. 1970. High temperature flow of dunite and peridotite. *Geological Society of America Bulletin* 81:2181–2202.

Changela H. G. and Bridges J. C. 2011. Alteration assemblages in the nakhlites: Variation with depth on Mars. *Meteoritics & Planetary Science* 45:1847–1867.

Chatzitheodoridis E., Haigh S., and Lyon I. 2014. A conspicuous clay ovoid in Nakhla: Evidence for subsurface hydrothermal alteration on Mars with implications for astrobiology. *Astrobiology* 14:651–693.

Childs C. W. 1992. Ferrihydrite—A review of the structure, properties and occurrence in relation to soils. *Zeitschrift für Pflanzenernährung und Bodenkunde* 155:441–448.

Cohen B. E., Mark D. F., Cassata W. S., Lee M. R., Tomkinson T., and Smith C. L. 2017. Taking the pulse of Mars via dating of a plume-fed volcano. *Nature Communications* 8:640.

Corrigan C. M., Velbel M. A., and Vicenzi E. P. 2015. Modal abundances of pyroxene, olivine, and mesostasis in nakhlites: Heterogeneity, variation, and implications for nakhlite emplacement. *Meteoritics & Planetary Science* 50:1497–1511.

Coulson I. M., Beech M., and Nie W. 2007. Physical properties of Martian meteorites: Porosity and density measurements. *Meteoritics & Planetary Science* 42:2043–2054.

Day J. M. D., Taylor L. A., Floss C., and McSween H. Y. 2006. Petrology and chemistry of MIL 03346 and its significance in understanding the petrogenesis of nakhlites on Mars. *Meteoritics & Planetary Science* 41:581–606.

Deer W. A., Howie R. A., and Zussman J. 1992. *An introduction to the rock-forming minerals*, 2nd ed. London: Longman Scientific & Technical. 696 p.

Donnelly T., Waldron S., Tait A., Dougans J., and Bearhop S. 2001. Hydrogen isotope analysis of natural abundance and deuterium-enriched waters by reduction over chromium on-line to a dynamic dual inlet isotope-ratio mass spectrometer. *Rapid Communications in Mass Spectrometry* 15:1297–1303.

Dreibus G., Palme H., Rammensee W., Spettel B., Weckwerth G., and Wänke H. 1982. Composition of the Shergotty parent body: Further evidence of a two-component model for planet formation (abstract). 13th Lunar and Planetary Science Conference. p. 186.

Forman L., Bland P., Timms N. E., Collins G., Davison T., Ciesla F., Benedix G., Daly L., Trimby P., and Yang L. 2016. Hidden secrets of deformation: Impact-induced compaction within a CV chondrite. *Earth and Planetary Science Letters* 452:133–145.

Forman L., Bland P., Timms N. E., Daly L., Benedix G., Trimby P., Collins G., and Davison T. 2017. Defining the mechanism for compaction of the CV chondrite parent body. *Geology* 45:559–562.

Friedman-Lentz R. C., Taylor G. J., and Treiman A. H. 1999. Formation of a Martian pyroxenite: A comparative study of the nakhlite meteorites and Theo's Flow. *Meteoritics & Planetary Science* 34:919–932.

Fritz J., Artemieva N., and Greshake A. 2005. Ejection of Martian meteorites. *Meteoritics & Planetary Science* 40:1393–1411.

Garenne A., Beck P., Montes-Hernandez G., Chiriac R., Toche F., Quirico E., Bonal L., and Schmitt B. 2014. The abundance and stability of "water" in type 1 and 2 carbonaceous chondrites (CI, CM and CR). *Geochimica et Cosmochimica Acta* 137:93–112.

Gillet P., Barrat J. A., Deloule E., Wadhwa M., Jambon A., Sautter V., Devouard B., Neuville D., Benzerara K., and Lesourd M. 2002. Aqueous alteration in the Northwest Africa 817 (NWA 817) Martian meteorite. *Earth and Planetary Science Letters* 203:431–444.

Gooding J. L., Wentworth S. J., and Zolensky M. E. 1991. Aqueous alteration of the Nakhla meteorite. *Meteoritics* 26:135–143.

Goodrich C. A., Treiman A. H., Filiberto J., Gross J., and Jercinovic M. 2013. K_2O-rich trapped melt in olivine in the Nakhla meteorite: Implications for petrogenesis of nakhlites and evolution of the Martian mantle. *Meteoritics & Planetary Science* 48:2371–2405.

Grossman J. N. and Zipfel J. 2001. The Meteoritical Bulletin, No. 85. *Meteoritics & Planetary Science* 36:A293–A322.

Hallis L. J. and Taylor G. J. 2011. Comparisons of the four Miller Range nakhlites, MIL 03346, 090030, 090032 and 090136: Textural and compositional observations of primary and secondary mineral assemblages. *Meteoritics & Planetary Science* 46:1787–1803.

Hallis L. J., Taylor G. J., Nagashima K., Huss G. R., Needham A. W., Grady M. M., and Franchi I. A. 2012. Hydrogen isotope analyses of alteration phases in the

nakhlite Martian meteorites. *Geochimica et Cosmochimica Acta* 97:105–119.

Hallis L. J., Ishii H. A., Bradley J. P., and Taylor G. J. 2014. Transmission electron microscope analyses of alteration phases in MIL 090030. *Geochimica et Cosmochimica Acta* 134:275–288.

Hallis L. J., Kemppinen L., Lee M., and Taylor L. A. 2017. The origin of alteration "orangettes" in shergottite Dhofar 019. *Meteoritics & Planetary Science* 52:2695–2706.

Hicks L. J., Bridges J. C., and Gurman S. J. 2014. Ferric saponite and serpentine in the nakhlite Martian meteorites. *Geochimica et Cosmochimica Acta* 136:194–210.

Imae N. and Ikeda Y. 2007. Petrology of the Miller Range 03346 nakhlite in comparison with the Yamato-000593 nakhlite. *Meteoritics & Planetary Science* 42:171–184.

Jambon A., Sautter V., Barrat J.-A., Gattacceca J., Rochette P., Boudouma O., Badia D., and Devouard B. 2016. Northwest Africa 5790: Revisiting nakhlite petrogenesis. *Geochimica et Cosmochimica Acta* 190:191–212.

Jung H. and Karato S.-I. 2001. Water-induced fabric transitions in olivine. *Science* 293:1460–1463.

Karato S.-I., Jung H., Katayama I., and Skemer P. 2008. Geodynamic significance of seismic anisotropy of the upper mantle: New insights from laboratory studies. *Annual Review of Earth and Planetary Sciences* 36:59–95.

Karlsson H. R., Clayton R. N., Gibson E. K. Jr., and Mayeda T. K. 1992. Water in SNC meteorites: Evidence for a Martian hydrosphere. *Science* 255:1409–1411.

Kendrick J. L. and Jamieson R. A. 2016. The fate of olivine in the lower crust: Pseudomorphs after olivine in coronitic metagabbro from the Grenville Orogen, Ontario. *Lithos* 260:356–370.

Kuebler K. E. 2013. A combined electron microprobe (EMP) and Raman spectroscopic study of the alteration products in Martian meteorite MIL 03346. *Journal of Geophysical Research Planets* 118:347–368.

Kuebler K., Jolliff B. L., Wang A., and Haskin L. A. 2004. A survey of olivine alteration products using Raman spectroscopy (abstract #1704). 35th Lunar and Planetary Science Conference. CD-ROM.

Lécuyer C., Gillet P., and Robert F. 1998. The hydrogen isotope composition of seawater and the global water cycle. *Chemical Geology* 145:249–261.

Lee M. R. and Bland P. A. 2004. Mechanisms of weathering of meteorites recovered from hot and cold deserts and the formation of phyllosilicates. *Geochimica et Cosmochimica Acta* 68:893–916.

Lee M. R. and Chatzitheodoridis E. 2016. Replacement of glass in the Nakhla meteorite by berthierine: Implications for understanding the origins of aluminum-rich phyllosilicates on Mars. *Meteoritics & Planetary Science* 51:1643–1653.

Lee M. R. and Lindgren P. 2016. Aqueous alteration of chondrules from the Murchison CM carbonaceous chondrite: Replacement, pore filling, and the genesis of polyhedral serpentine. *Meteoritics & Planetary Science* 51:1003–1021.

Lee M. R. and Smith C. L. 2006. Scanning transmission electron microscopy using a SEM: Applications to mineralogy and petrology. *Mineralogical Magazine* 70:561–572.

Lee M. R., Bland P. A., and Graham G. 2003. Preparation of TEM samples by focused ion beam (FIB) techniques: Applications to the study of clays and phyllosilicates in meteorites. *Mineralogical Magazine* 67:581–592.

Lee M. R., Tomkinson T., Mark D. F., Stuart F. M., and Smith C. L. 2013. Evidence for silicate dissolution on Mars from the Nakhla meteorite. *Meteoritics & Planetary Science* 48:224–240.

Lee M. R., MacLaren I., Andersson S. M. L., Kovacs A., Tomkinson T., Mark D. F., and Smith C. L. 2015a. Opal-A in the Nakhla meteorite: A tracer of ephemeral liquid water in the Amazonian crust of Mars. *Meteoritics & Planetary Science* 50:1362–1377.

Lee M. R., Tomkinson T., Hallis L. J., and Mark D. F. 2015b. Formation of iddingsite veins in the Martian crust by centripetal replacement of olivine: Evidence from the nakhlite meteorite Lafayette. *Geochimica et Cosmochimica Acta* 154:49–65.

Leshin L. A. and Vicenzi E. 2006. Aqueous processes recorded by Martian meteorites: Analyzing Martian water on Earth. *Elements* 2:157–162.

Leshin L. A., Epstein S., and Stolper E. M. 1996. Hydrogen isotope geochemistry of SNC meteorites. *Geochimica et Cosmochimica Acta* 60:2635–2650.

McCarthy T. S., Erlank A. J., Willis J. P., and Ahrens L. H. 1974. New chemical analyses of six achondrites and one chondrite. *Meteoritics* 9:215–222.

McCubbin F. M., Elardo S. M., Shearer C. K. Jr., Smirnov A., Hauri E. H., and Draper D. S. 2013. A petrogenetic model for the comagmatic origin of chassignites and nakhlites: Inferences from chlorine-rich minerals, petrology, and geochemistry. *Meteoritics & Planetary Science* 48:819–853.

McSween H. Y. Jr. 1994. What we have learned about Mars from SNC meteorites. *Meteoritics* 29:757–779.

Meunier A., Petit S., Ehlmann B. L., Dudoignon P., Westall F., Mas A., Albani A., and Ferrage E. 2012. Magmatic precipitation as a possible origin of Noachian clays on Mars. *Nature Geoscience* 5:739–743.

Mikouchi T., Miyamoto M., Koizumi E., Makishima J., and McKay G. 2006. Relative burial depths of nakhlites: An update (abstract #1865). 37th Lunar and Planetary Science Conference. CD-ROM.

Mikouchi T., Makishima J., Kurihara T., Hoffmann V. H., and Miyamoto M. 2012. Relative burial depth of nakhlites revisited (abstract #2363). 43rd Lunar and Planetary Science Conference. CD-ROM.

Mustard J. F., Murchie S. L., Pelkey S. M., Ehlmann B. L., Milliken R. E., Grant J. A., Bibring J.-P., Poulet F., Bishop J., Dobrea E. N., Roach L., Seelos F., Arvidson R. E., Wiseman S., Green R., Hash C., Humm D., Malaret E., McGovern J. A., Seelos K., Clancy T., Clark R., Marais D. D., Izenberg N., Knudson A., Langevin Y., Martin T., McGuire P., Morris R., Robinson M., Roush T., Smith M., Swayze G., Taylor H., Titus T., and Wolff M. 2008. Hydrated silicate minerals on Mars observed by the Mars reconnaissance orbiter CRISM instrument. *Nature* 454:305–309.

Noguchi T., Nakamura T., Misawa K., Imae N., Aoki T., and Toh S. 2009. Laihunite and jarosite in the Yamato 00 nakhlites: Alteration products on Mars? *Journal of Geophysical Research* 114:E10004.

Nyquist L. E., Bogard D. D., Shih C.-Y., Greshake A., Stöffler D., and Eugster O. 2001. Ages and geologic histories of Martian meteorites. In *Chronology and evolution of Mars.*, edited by Kallenbach R., Geiss J., and

Hartmann W. K. Dordrecht, the Netherlands: Kluwer Academic Publishers. pp. 105–164.

Prior D. J., Mariani E., and Wheeler J. 2009. EBSD in the Earth sciences: Applications, common practice, and challenges. In *Electron backscatter diffraction in materials science*, edited by Schwartz A. J., Kumar M., Adams B. L., and Field D. P. New York: Springer. pp. 345–360.

Richter F., Chaussidon M., Mendybaev R., and Kite E. 2016. Reassessing the cooling rate and geologic setting of Martian meteorites MIL 03346 and NWA 817. *Geochimica et Cosmochimica Acta* 182:1–23.

Sautter V., Barrat J. A., Jambon A., Lorand J. P., Gillet P., Javoy M., Joron J. L., and Lesourd M. 2002. A new Martian meteorite from Morocco: The nakhlite North West Africa 817. *Earth and Planetary Science Letters* 195:223–238.

Sautter V., Jambon A., and Boudouma O. 2006. Cl-amphibole in the nakhlite MIL 03346: Evidence for sediment contamination in a Martian meteorite. *Earth and Planetary Science Letters* 252:45–55.

Stelzner T., Heide K., Bischoff A., Weber D., Scherer P., Schultz L., Happel M., Schron W., Neupert U., Michel R., Clayton R. N., Mayeda T. K., Bonani G., Haidas I., Ivy-Ochs S., and Suter M. 1999. An interdisciplinary study of weathering effects in ordinary chondrites from the Acfer region, Algeria. *Meteoritics & Planetary Science* 34:787–794.

Tomkinson T., Lee M. R., Mark D. F., and Smith C. L. 2013. Sequestration of Martian CO_2 by mineral carbonation. *Nature Communications* 4:2662.

Tomkinson T., Lee M. R., Mark D. F., Dobson K. J., and Franchi I. A. 2015. The Northwest Africa (NWA) 5790 meteorite: A mesostasis-rich nakhlite with little or no Martian aqueous alteration. *Meteoritics & Planetary Science* 50:287–304.

Treiman A. H. 2005. The nakhlite meteorites: Augite-rich igneous rocks from Mars. *Chemie der Erde* 65:203–270.

Treiman A. H. and Lindstrom D. J. 1997. Trace element geochemistry of Martian iddingsite in the Lafayette meteorite. *Journal of Geophysical Research* 102:9153–9163.

Treiman A. H., Barrett R. A., and Gooding J. L. 1993. Preterrestrial aqueous alteration of the Lafayette (SNC) meteorite. *Meteoritics* 28:86–97.

Usui T., Alexander C. M. O'D., Wang J. H., Simo J. I., and Jones J. H. 2012. Origin of water and mantle-crust interactions on Mars inferred from hydrogen isotopes and volatile element abundances of olivine-hosted melt inclusions of primitive shergottites. *Earth and Planetary Science Letters* 357–358:119–129.

Usui T., Alexander C. M. O'D., Wang J., Simon J. I., and Jones J. H. 2015. Meteoritic evidence for a previously unrecognized hydrogen reservoir on Mars. *Earth and Planetary Science Letters* 410:140–151.

Velbel M. A. 2012. Aqueous alteration in Martian meteorites: Comparing mineral relations in igneous-rock weathering of Martian meteorites and in the sedimentary cycle of Mars. In *Sedimentary geology of Mars*, edited by Grotzinger J. and Milliken R. Tulsa, Oklahoma: Society for Sedimentary Geology Special Publication. pp. 97–117.

Vicenzi E. P., Fisk M. R., Treiman A., and Wilson S. 2002. Comparison of clay minerals produced during low-temperature alteration of mafic rocks from Earth and Mars. *Meteoritics & Planetary Science* 37:A144–A144.

Warke P. A. and Smith B. J. 1998. Effects of direct and indirect heating on the validity of rock weathering simulation studies and durability tests. *Geomorphology* 22:347–357.

Watt L. E., Bland P. A., Prior D. J., and Russell S. S. 2006. Fabric analysis of Allende matrix using EBSD. *Meteoritics & Planetary Science* 41:989–1001.

Webster C. R., Mahaffy P. R., Flesch G. J., Niles P. B., Jones J. H., Leshin L. A., Atreya S. K., Stern J. C., Christensen L. E., Owen T., Franz H., Pepin R. O., and Steele A., and the MSL Science Team. 2013. Isotope ratios of H, C, and O in CO_2 and H_2O of the Martian atmosphere. *Science* 341:260–263.

Wogelius R. A. and Walther J. V. 1992. Olivine dissolution kinetics at near-surface conditions. *Chemical Geology* 97:101–112.